Journal of Molecular Structure 1250 (2022) 131834

Contents lists available at ScienceDirect

Journal of Molecular Structure

journal homepage: www.elsevier.com/locate/molstr

Molecular structure, quantum chemical and spectroscopic properties of 2,6–dibromonaphthalene by density functional theory calculations

Tevfik Raci Sertbakan*, Fatmanur Özçelik

Kırşehir Ahi Evran University, Art and Science Faculty, Department of Physics, KIRŞEHİR, Turkey

ARTICLE INFO

Article history:
Received 15 May 2021
Revised 25 October 2021
Accepted 28 October 2021
Available online 5 November 2021

Keywords:
2,6–Dibromonaphthalene
DFT
Vibrational spectra
NMR spectra
UV/visible spectra
HOMO-LUMO

ABSTRACT

In this work, the quantum chemical calculations were performed by means of the Gaussian09 packet program, using DFT in gas phase at the B3LYP level, with cc-pVDZ, cc-pVTZ, 6-31G(d,p) and 6-311G(d,p) basis sets. The most stable conformation of the 2,6–dibromonaphthalene (2,6–DBrN) molecule in free state was determined by the Spartan'14 program. The vibrational frequencies have been calculated at the same level of theory. These frequencies were calculated and scaled, and then values have been compared with the experimental Infrared and Raman spectra. The vibrational modes were determined based on TED analysis on the basis of 6-311G(d,p) using the SQM program. Theoretical ^{13}C–NMR and ^{1}H–NMR chemical shifts of the 2,6–DBrN molecule were calculated in DMSO and were compared the experimental values. NBO analysis study of 2,6–DBrN was performed to investigate charge transfer as well as to analyzed intra- and interactions. The HOMO and LUMO energy levels of the 2,6–DBrN molecule were determined. Besides, molecular electrostatic potential (MEP) maps of the studied molecule were made using the DFT method. Since the apparent absorption maxima of the molecules correspond to the electron transitions between the boundary orbitals corresponding to the HOMO–LUMO energies, these transitions were analyzed by UV/Visible spectroscopy.

© 2021 Elsevier B.V. All rights reserved.

1. Introduction

Naphthalene derivatives are molecules that can be found in different plant species and have a wide range of applications. Some of these applications can be listed as material science, pharmacology and biology [1]. They are also used in the food, cosmetic and fabric industries. They are also used in the health sector in the treatment of antitumor, anti-inflammatory, antimicrobial and even cancer [2]. Therefore, spectroscopic characterization of these naphthalene derivatives is very important [2–8]. The 2,6–dibromonaphthalene (2,6–DBrN) molecule we used in this study causes skin irritation, severe eye damage, respiratory irritation and is toxic to aquatic life with long-lasting effects. This molecule can be considered as an important molecule that can be used in medicine as a naphthalene derivative. So, quantum chemical and spectroscopic studies of this molecule could aid medical studies. The destruction of cancer cells can be thanks to such toxic molecules [9]. This may be possible by targeting naphthalene derivatives to their biomolecules and using small amounts [10]. It can be predicted that the molecule used in this study may also be used against cancer cells in the future. That's why we have done this study with this molecule.

Although there is no X–ray study that gives the exact structure of the 2,6–DBrN molecule, there are many spectroscopic studies related to similar molecules [11–18]. However, the X–ray study related to a molecule similar to the molecule we studied was found and geometric parameters were given in comparison with this molecule, naphthalene derivatives [11–13]. In addition, one of these spectroscopic studies is the 1,4–dibromonaphthalene molecule. This molecule is very similar to title molecule. In this study, the authors analyzed the Raman spectrum of 1,4–DBrN theoretically and experimentally. Another study we use to discuss vibrational frequencies is the work of Geetha et al. [14]. The vibrational frequency studies of 2,6–DBrN molecule were carried out by FT–IR and FT–Raman Spectroscopy in comparison with this naphthalene derivative study. The experimental and theoretical investigations were carried out in these two spectroscopic branches. In this study, NMR and UV/Visible region spectroscopy studies were also conducted experimentally and theoretically. The NBO method, which is a structural analysis method in molecules, was also made in this study. Finally, HOMO and LUMO molecular orbital energy

* Corresponding author.
E-mail address: trsertbakan@ahievran.edu.tr (T.R. Sertbakan).

https://doi.org/10.1016/j.molstruc.2021.131834
0022-2860/© 2021 Elsevier B.V. All rights reserved.

levels and molecular electrostatic potential maps have been studied. Details of all these studies will be explained in order.

2. Experimental details

The 2,6–DBrN molecule was purchased from Sigma-Aldrich. The FT–IR spectrum of the molecule was taken by pellet method in the KBr window at 4000–400 cm^{-1} region at room temperature using Perkin-Elmer Spectrum One FT–IR spectrometer. Then, the Fig. 8 Raman spectrum of 2,6–DBrN molecule was taken using a Thermo Scientific DXR Raman Microscope with Nd: YVO4 DPSS Raman Spectrophotometer, which was stimulated with 532 nm laser at 4000–50 cm^{-1} region. ^{1}H and ^{13}C NMR spectra were taken in dimethylsulfoxide (DMSO) solution in a tetramethylsilane (TMS) calorimeter at 25 °C using a Bruker DPX 400 MHz NMR spectrometer. Finally, the UV/visible absorption spectrum of title molecule is given in diluted DMSO solution. Experimentally, a solution in dimethylsulfoxide (DMSO) solvent was prepared first to obtain the UV/Visible spectrum of our sample. This solution was obtained by placing 1 ml in a 10^{-4} molar 2,6–DBrN container and completing it in 10 ml with DMSO. The UV/Vis spectrometer we use is Shimadzu trademark, UV–1800 240 V SOFT model spectrometer.

3. Computational details

In the present work, we optimized the molecular structure of 2,6–DBrN using B3LYP/6-311G(d,p) basis set. The shape of this molecule with geometric optimization is given in Fig. 1. Geometric parameters of the molecule such as bond lengths, bond angles and dihedral angles were calculated using Density Functional Theory (DFT) at the B3LYP level, with cc-pVDZ, cc-pVTZ, 6-31G(d,p) and 6-311G(d,p) basis sets [19]. Using the same method and basis sets in DFT, title molecule's vibration frequencies were calculated and then multiplied by scale factors and presented in a table. In addition, the vibrational modes are assignment by TED analysis using the SQM program [20]. These vibrational frequencies obtained were compared with their experimental values. Some reference structures in which we compare the geometric parameters and vibrational frequencies of 2,6–DBrN molecule are shown in Fig. 1.

NBO analysis is an important tool that provides a useful resource to learn intra-molecular interactions, interactions between molecules and bonds. At the same time, this analysis is a convenient way to investigate charge transfer or conjugate interactions in molecular systems [21]. In order to make these explanations, we also carried out NBO analysis studies of 2,6–DBrN molecule. The HOMO and LUMO values of a molecule enable the determination of the distribution of electrons on the molecular orbitals. While the HOMO energy of the molecule is related to its ionization potential, LUMO energy is related to electron affinity [22,23]. The HOMO and LUMO energy values of the 2,6–DBrN molecule were calculated in the cc-pVDZ basis set of the B3LYP method. The molecular electrostatic potential (MEP) relates to electron density and is a very useful descriptor for us to understand hydrogen bond interactions as well as electrophilic and nucleophilic reactions of regions [24,25]. We drew the MEP maps of the molecule with the same method and basis set. Then, the UV/Visible absorption spectrum of the 2,6–DBrN molecule was taken in diluted DMSO solution. The wavelength (λ_{max}) at which the molecule absorbed the maximum was found to be 280 nm. Scanning of this molecule includes bands in the wavelength range from 210 to 330 nm. ^{1}H and ^{13}C NMR isotropic protective tensors of the 2,6–DBrN molecule were studied using the GIAO method [26,27], one of the most common approaches in calculating nuclear magnetic shielding tensors. All calculations were made with the Gaussian09 package program [19].

4. Results and discussion

4.1. Geometric parameters

The geometrical structure parameters of the 2,6–DBrN molecule were theoretically calculated by considering the most stable structure of the molecules. These calculated parameters are given in Table S1 in comparison with the X–ray studies of three different molecules similar to the molecule we are working on. Calculated geometric parameter values are quite compatible with values in reference studies. However, some minor differences are observed between the calculated and referenced geometric parameters. One of the reasons for this is that while we have calculated the molecule in the gas phase, 1,5–dibromonaphthalene (1.5–DBrN) and 1,8–dibromonaphthalene (1.8–DBrN) molecules are in the solid phase in the reference X–ray studies [12]. Another reason for the very small differences that emerge may be the places of binding of the Bromine atom to the Naphthalene molecule and, of course, these parameters change slightly with the change of the center of mass of the molecule. In addition, when we look at the structure of XX Wu et al. [13] in their study with the 3,6–dibromonaphthalene–2,7diylbis(trifluoromethanesulfonate) (3,6–DBrN–2,7–diol) molecule, we see that there are atoms other than title molecule that have other properties such as oxygen, sulfur and fluorine. As seen in this study, it can be said that another reason for the small differences in the experimental–theory comparison in geometric parameters is the change in the center of mass.

The bond length between the C_1–C_2 and C_{10}–C_{13} atoms in the 2,6–DBrN molecule was calculated in the basis sets studied in the B3LYP method as follows: cc-pVDZ 1.377 Å, cc-pVTZ 1.368 Å, 6–31G(d,p) 1.374 Å, 6–311G(d,p) 1.371 Å. It can be seen from **Table S1** that these bond length values are compatible with the reference structure values. Similar bond length values are also seen between the atoms C_1–C_6 and C_{13}–C_{14}.

The bond length similarity above is also present in C–H and C–Br bonds. In reference structures, the lengths of these bonds are in harmony with the values we calculate.

The angle values between the C_2–C_1–C_6 (C_{14}–C_{13}–C_{10}) atoms in the 2,6–DBrN molecule were calculated B3LYP/cc-pVDZ 121^0.557, cc-pVTZ 121^0.587, 6-311G(d,p) 121^0.665 methods and basis sets. Similarly, the angle between the C_1–C_2–C_3 (C_{13}–C_{10}–C_4) atoms in the 2,6–DBrN molecule B3LYP/cc-pVDZ 119^0.802, cc-pVTZ 119^0.826, 6-31G(d,p) 119^0.791, 6-311G(d,p) 119^0.751 calculated for method and basis sets.

Apart from these angles we have chosen, Table S1 shows that the results are compatible for all the basis sets calculated in the B3LYP method. Looking at the method and basis sets calculated at four angles between the two bromine atoms and carbon atoms in 2,6–DBrN molecule, the results are quite consistent. The same agreement applies to all dihedral angles in this molecule.

We discussed some of the geometric parameters we calculated for the 2,6–DBrN molecule. The calculated values of these parameters were also compared with the values in the reference studies [11–13] and they were found to be compatible. For small differences in these values, the reasons can be interpreted as described above.

After all, the angle between the C–C–C bonds in the benzene ring is 120°, this molecule is planar. The same bonds are also 180° for the naphthalene molecule consisting of two benzene. We have confirmed this result in our accounts. In other words, we can say that the naphthalene ring and its molecule formed by attaching two bromides to this ring retains its flatness as a result of these angles calculated. The values of the dihedral angles we calculated for the 2,6–DBrN molecule also confirm this interpretation. In other words, dihedral angles in this molecule were calculated

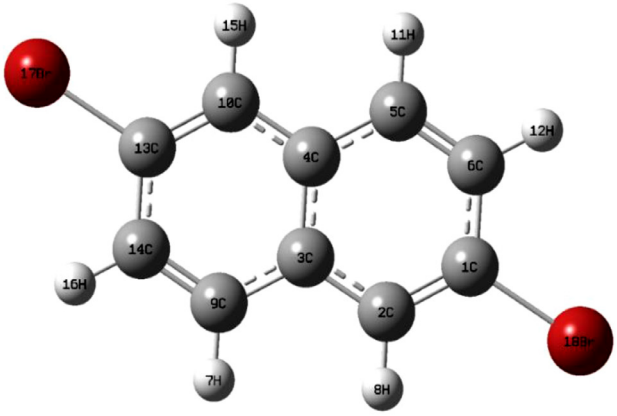

Optimized 2,6–dibromonaphthalene molecule

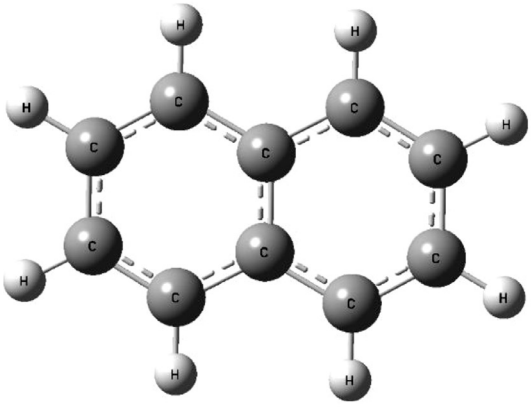

The Naphthalene molecule

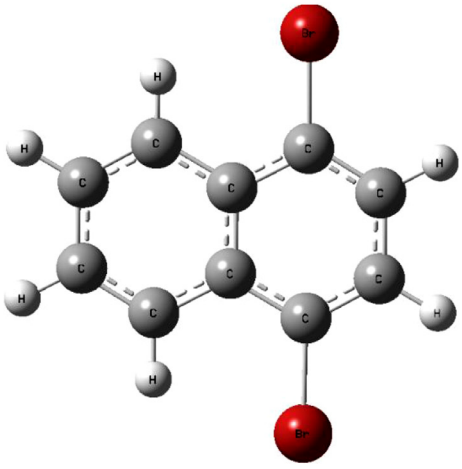

The 1,4–dibromonaphthalene molecule

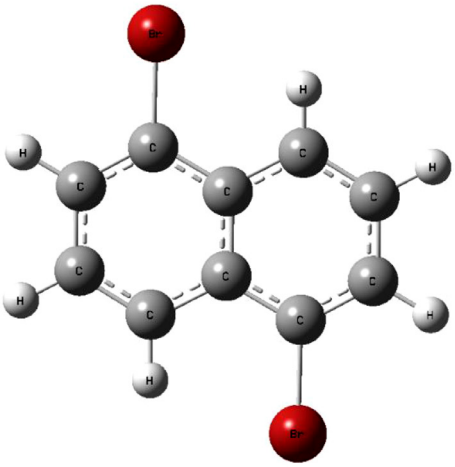

The 1,5–dibromonaphthalene molecule

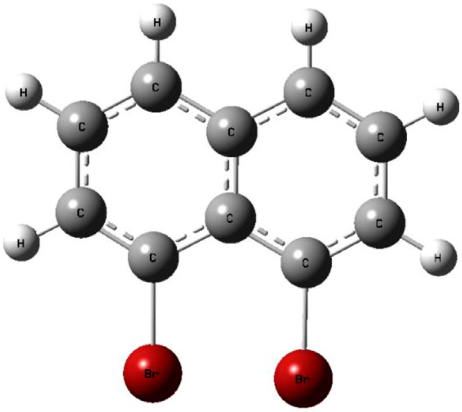

The 1,8–dibromonaphthalene molecule

Fig. 1. Optimized 2,6–dibromonaphthalene molecule and some naphthalene derivative molecules used as reference.

Table 3
The correlation coefficients for calculated vibration frequencies.

Method / Basis Set	Correlation coefficients – R^2 (FT-IR)	Correlation coefficients – R^2 (FT-Raman)
B3LYP/cc-pVDZ	0.9970	0.9976
B3LYP/ cc-pVTZ	0.9970	0.9974
B3LYP/6-31G(d,p)	0.9969	0.9977
B3LYP/6-311G(d,p).	0.9969	0.9974

at 0^0 and 180^0 degrees. When we compare the angles we calculated with the dihedral angles of the reference molecule, it is seen that the deviations are very small. The reason for this is that as we explained above, we can say that they are different heavy groups that attach to the reference molecule.

When we look at all these geometric parameters (bond lengths and angles between bonds) we calculated for the 2,6–DBrN molecule, it can be said that cc-pVDZ is the basis set that gives the best results among the four basis sets we used. In other words, the calculations made with the cc-pDVZ basis set gave results closer to the experimental values. In our opinion, this is because the more appropriate of these basis sets, which takes into account the atomic orbitals of the atoms 2,6–DBrN molecule has, is cc-pDVZ.

4.2. Vibrational assignments

Since the 2,6–DBrN molecule has a non-linear structure with 18 atoms, there are 48 vibration modes. This molecule has a C_{2h} point group considering its shape and symmetry elements. The symmetry types corresponding to a vibration each of the C_{2h} point group are A_g, B_g, A_u and B_u. After analyzing the mod for this molecule, we have given the total number of vibrations we have obtained according to symmetry types as follows.

$$\Gamma_{3N} = 18A_g + 9B_g + 9A_u + 18\ B_u$$

$$\Gamma_{rotation} = A_g + 2B_g$$

$$\Gamma_{translation} = A_u + 2B_u$$

$$\Gamma_{vibration} = \Gamma_{3N} - (\Gamma_{translation} + \Gamma_{rotation})$$

$$\Gamma_{vibration} = 17A_g + 7B_g + 8A_u + 16B_u$$

Thus, we distinguished 48 vibrations according to symmetry types. The normal vibration modes of the 2,6–DBrN molecule are calculated in four basis sets in B3LYP method and scaled vibration frequencies, theoretical IR & Raman vibration frequency values and peak intensities are given in Table S2. TED results are also provided in the same table to assignment vibrations. In Table S2, calculated normal vibration modes, scaled vibration frequencies, IR and Raman vibration frequencies of the 2,6–DBrN molecule are given. The values of the experimental IR and Raman vibration frequencies of the 2,6–DBrN molecule are also given in the same table. In addition, experimental and calculated FTIR and Raman spectra of the 2,6–DBrN molecule were taken and given in the Fig. 2 and Fig. S3.

Good linearity between the vibration frequencies calculated and experimentally measured for the 2,6-DBrN molecule was determined by the correlation coefficients (R^2) found for all methods and basis sets studied (Table 3). The small differences observed in the calculation of the correlation coefficients may be due to the formation of intermolecular hydrogen bonds [28]. In addition, these frequency values are in the solid phase in the experimental measurement, while in the gas phase in the theoretical calculations. This may be one reason for the small differences.

When we look at the correlation coefficients in Table 3, it is seen that the method/basis set closest to the experimental result is B3LYP/cc-pVDZ. The correlation graphics drawn for the 2,6–DBrN molecule are given in Fig. S4 (for Infrared Spectra) and Fig. S5(for Raman Spectra).

Since there are no studies in the literature involving the vibrations of the 2,6–DBrN molecule, we compared the vibrations of this molecule with the work of other similar molecules. Two of these studies are related to the pure naphthalene molecule that has no bromine atom bound [15,16]. In order to enrich this study, vibration frequencies studies made with naphthalene derivatives are also given as reference (Table S2,) [14,17]. The Raman spectrum of the naphthalene was previously reported by McClellan [15]. As a result, they gave Raman shifts of this molecule. Lippincott and O'Reilly Jr made both IR and Raman studies of naphthalene molecule in reference 16. In the naphthalene derivatives studies, Michaelian, Ziegler [17] and Geetha et al. [14] gave the results of the Raman spectrum studies of the 1,4–dibromonaphthalene molecule.

As seen from the table, the frequency values obtained by multiplying the scale factors are very compatible with the experimental values. In addition, when the vibrations of the 2,6–DBrN molecule were compared with the reference molecule vibrations, the same agreement was observed.

4.2.1. Ring vibrations

The naphthalene molecule consists of two benzene molecules. Therefore, we must start the vibrational frequencies of title molecule with the vibrations of the benzene molecule. The benzene rings have six equal C–C bonds, so there will be six C–C strain vibrations. In addition, benzene rings have both in-plane and out-of-plane C–C–C bending vibrations. However, in the study of the 2–methoxy–4–nitroaniline molecule, it has been noted that these vibrations are inactive in the IR spectrum due to symmetry [29]. In general, C–C stretching vibrations in aromatic compounds are observed in the region of 1430–1650 cm^{-1}. The C–C stretching vibration in the 1,4-dibromonaphthalene molecule was observed in the region of 1616–1256 cm^{-1} (vib. mod.: 34–42) [11]. In our 2,6–DBrN molecule, the C–C stretching vibrations were calculated according to the basis sets as follows; cc-pVDZ basis set in the range of 1304–1614 cm^{-1}, cc-pVTZ basis set in the range of 1312–1594 cm^{-1}, 6-31G(d,p) basis set in the range of 1311–1605 cm^{-1}, 6-311G(d,p) in the basis set in the range of 1300–1587 cm^{-1} (Table S2).

Experimentally, these vibrations were observed in the range of 1346–1568 cm^{-1} in FT–IR and 1373–1613 cm^{-1} in FT–Raman. These vibrations in 1,4-dibromonaphtalene molecule was calculated at 1617, 1578 and 1524 cm^{-1} [14]. Also, these vibrations were observed in the normal Raman spectrum at 1616, 1583, 1521 cm^{-1} and in the SERS (Surface Enhanced Raman Spectroscopy) at 1604,1587 and 1534 cm^{-1} [14]. In-plane C–C–C bending vibration frequencies in the ring are always observed in the region of 1000–600 cm^{-1} in the mid–IR region [30]. The experimentally observed frequency values for these vibrations of the 2,6–DBrN molecule are 938–624 cm^{-1}. C–C–C bending vibration frequencies for this molecule were calculated between 920 and 625 cm^{-1}. When we look at the vibration frequencies in this angle bending region, the

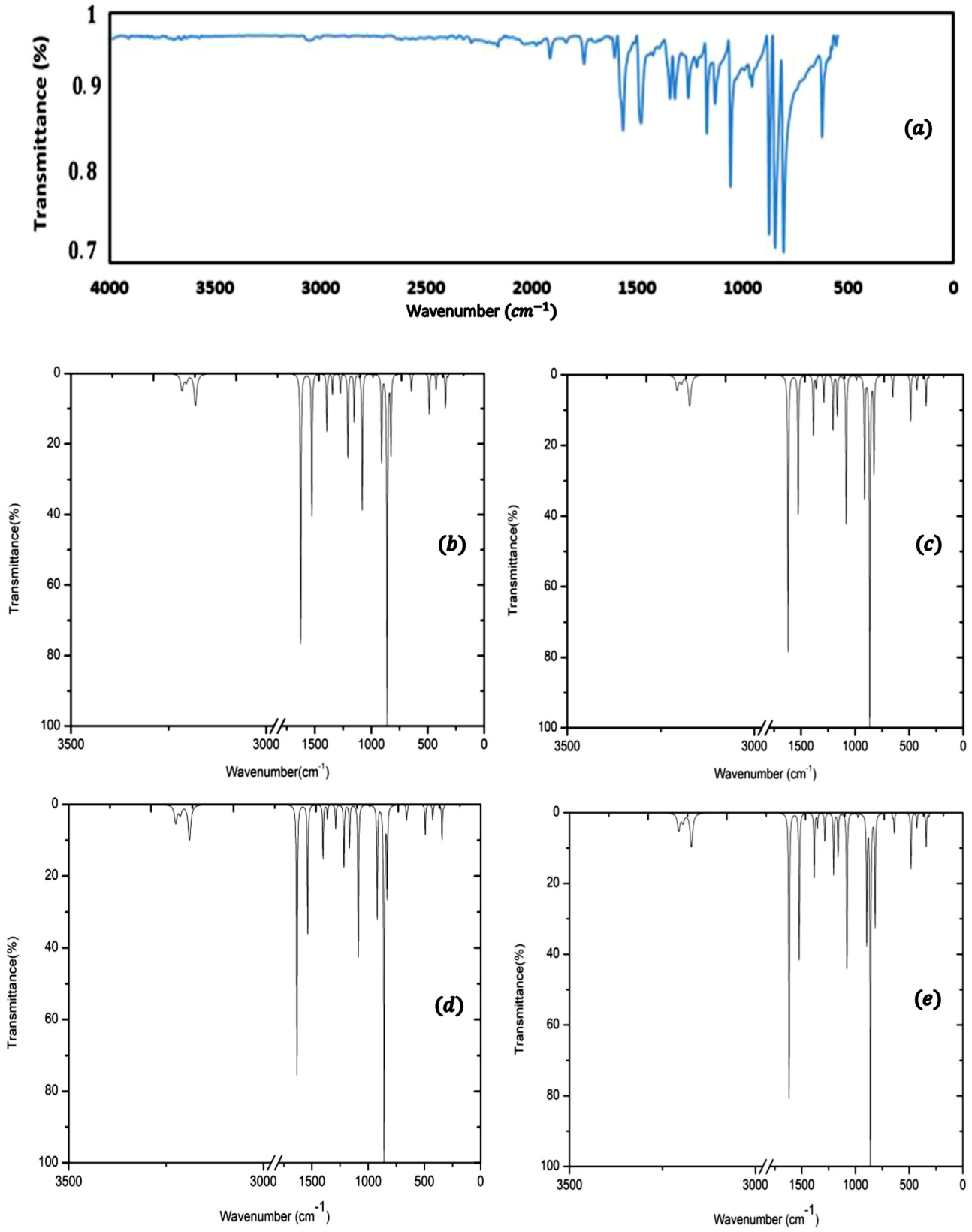

Fig. 2. The experimental (a) and the theoretical (B3LYP/cc-pVDZ (b), B3LYP/cc-pVTZ (c), B3LYP/6-31G(d,p) (d) and B3LYP/6-311G(d,p) (e) basis sets) FT–IR spectra of the 2,6–dibromonaphthalene molecule, respectively.

theory-experiment result consistency can be observed. The reference comparison can also be made for these vibrations. As a result, the same harmony was observed.

4.2.2. C–H vibrations

As observed in similar studies to date, aromatic C–H bond stretching vibrations have been observed in the spectra in the frequency range of 3100–3000 cm^{-1} and in the form of weak intensity bands [31–33,21]. The reason for this can be said to be the reduction of negative charge by electron withdrawal from the carbon atom as a result of the inductive effect [21]. As a result, the dipole moment in the bonds will decrease and with this decrease the bond length will increase. The reduction of the bond length will also decrease the intensity of the vibration frequency [33]. In-plane and out-of-plane C–H bending vibration frequencies are observed in the regions of 1275–1000 cm^{-1} and 900–690 cm^{-1}, respectively [34,35]. The stretching and bending vibrations of the C–H bond of the 2,6–DBrN molecule in our study were observed experimentally in the Infrared and Raman spectra in these regions. Theoretically, B3LYP/cc-pVDZ, cc-pVTZ, 6-31G(d,p) and 6-311G(d,p) methods and basis sets showed vibration frequencies in the same regions (Table S2).

The stretching vibrations were calculated by B3LYP/cc-pVDZ in 3086–3119 cm^{-1} (vib. mod.: 43–48). In all these methods and basis sets, in-plane bending vibration frequencies were calculated in the region of 1328–1037 cm^{-1} (vib. mod.: 27–35), while out-of-plane angle bending frequencies were calculated in the region of 920–763 cm^{-1} (vib. mod.: 18–24) (Table S2). In addition, all these C–H vibration frequencies have been compared with the frequency values in our reference studies and a very good match has been achieved.

4.2.3. C–Br vibrations

The C–Br stretching mode of the massive bromine atom has been reported by Varsayni to the long wavelength portion of the Infrared region (200–480 cm^{-1}) [36]. In the 1,4–dibromonaphthalene molecule, this value was observed in the normal Raman spectrum at 383 cm^{-1} and 214 cm^{-1} and in the SERS at 381 and 237 cm^{-1} [14]. In addition, in the study related to the 2–bromo–4–methyl phenylamine molecule, two stretching vibrational frequencies are given, both in-plane and out-of-plane related to this bond. These values are; It is 262 cm^{-1} (in plane) and 182 cm^{-1} (out of plane) [37]. C–Br vibrations are also discussed in the work of Iramain et al. This study was done with 5–bromo–2–isonicoinoyl-trifluoroborate (B-ITFB) molecule. In the Raman spectrum of this molecule, the vibrational frequencies of carbon and bromine atoms are given as follows: 355 cm^{-1} (C–Br bond stretching vibration),284 cm^{-1} (C–Br in-plane deformation vibration), and 270 cm^{-1} (C–Br out-of-plane deformation vibration) [38]. Studies indicating ring deformation, ring torsion and wagging vibrations in the low frequency region are also available in the literature [39]. In our study, C–Br vibrational frequencies (vib. Mod: 5–8) in the 2,6-dibromonophthalene molecule were calculated as 174–333 cm^{-1}. Experimentally, we observed these vibrational frequencies only at 177 and 257 cm^{-1} in the FT–Raman spectrum. In the cc-PVDZ basis set, we marked the vibrations calculated at the frequency of 333 cm^{-1} as C–Br bond stretching, and the vibrations calculated at the frequencies of 251 cm^{-1} and 177 cm^{-1} as C–C–Br in-plane deformation vibrations (Table S2,). The reason for all these small differences in the experimentally observed and theoretically calculated vibrational frequencies of the 2,6–DBrN molecule is that the experimental measurements are in the solid phase and the theoretical calculations are in the gas phase; we can say. In addition, intermolecular hydrogen bonding may also cause these small differences [28].

Table 4
The experimental and theoretical NMR chemical shifts values of the carbon and hydrogen atoms of the 2,6–dibromonaphthalene molecule.

	B3LYP(Theoretical)				Experimental
	cc-pVDZ	cc-pVTZ	6-31G(d,p)	6-311G(d,p)	
H_8	7.942	8.170	8.744	8.132	8.265
H_{15}	7.942	8.170	8.744	8.132	8.265
H_7	7.837	8.006	8.695	7.997	7.911
H_{11}	7.837	8.006	8.695	7.997	7.911
H_{12}	7.631	7.756	8.445	7.745	7.721
H_{16}	7.631	7.756	8.445	7.745	7.721
	B3LYP(Theoretical)				Experimental
	cc-pVDZ	cc-pVTZ	6-31G(d,p)	6-311G(d,p)	
C_1	142.489	144.576	143.256	145.294	133.125
C_{13}	142.489	144.576	143.256	145.294	133.125
C_3	134.292	139.598	135.925	138.863	130.596
C_4	134.292	139.598	135.925	138.863	130.596
C_2	132.011	136.627	134.205	137.094	130.227
C_{10}	132.011	136.627	134.205	137.094	130.227
C_6	131.777	136.268	133.689	137.013	129.723
C_{14}	131.777	136.268	133.689	137.013	129.723
C_5	130.937	134.972	132.709	135.360	120.189
C_9	130.937	134.972	132.709	135.360	120.189

4.3. Nuclear magnetic resonance analysis

The Nuclear Magnetic Resonance technique, which calculates the isotropic chemical shifts, which is an effective way of accurately estimating the geometry of molecules and identifying organic compounds, also made important contributions in spectral marking. Using the density theory with experimental NMR spectrum analysis, the GIAO (Gauge Invariant Atomic Orbitals) approach [19,40] also provided scientists with the opportunity to comment further on this issue. Therefore, we made an NMR study using DFT/B3YLP/cc-pVDZ, cc-pVTZ, 6-31G(d,p), 6-311G(d,p) basis sets in order to comment on the 2,6–DBrN molecule. In this study, NMR spectra were obtained in DMSO solution in both experimental observation and theoretical calculation. The chemical shifts for calculated and observed ^{13}C and ^{1}H are given in Table 4. Peaks showing the experimental values in the NMR spectrum of this molecule in DMSO solution are given in Fig. S6 and Fig. S7. Calculated ^{13}C and ^{1}H absolute isotropic shielding parameters were converted to ^{13}C and ^{1}H chemical shifts.

$$\delta_{calculated} = \delta_{DMSO} - \delta_i$$

According to the electronic environment of the proton, chemical shifts in organic molecules differ greatly. The atom or group that is hydrogen–bonded or gives electrons near hydrogen increases shielding and moves the resonance towards a lower frequency. In contrast, the experimental NMR spectrum of hydrogen atoms for the 2,6-dibromonaphthalene molecule with electron withdrawing atoms or groups can reduce the protection and carry the resonance of the bound proton to a higher frequency [41]. The chemical shift values of the aromatic proton in the NMR spectrum of organic molecules are generally observed in the range of 7.00–8.00 ppm. In this study, chemical shifts signals of aromatic proton in the experimental NMR spectrum of the 2,6–DBrN molecule were observed in the range of 7.72–8.26 ppm. The same values were theoretically calculated in the range of 7.63–8.74 ppm.

When we look at the chemical shift values of all protons in this molecule, the two hydrogen atoms with the highest chemical shift (8.26 ppm) are H_8 and H_{15}. The reason for the high shifts for these two protons is the difference of the electronic environment, that is, the electron density is high. Two chemical shift values (H_{12}, H_{16}) for protons were observed in the NMR spectrum, which are the smallest values (7.72 ppm). The reason for these shifts may be the

solvent effects between the bromine atoms and the solvent DMSO molecule [42]. Experimental and theoretical chemical shift values are perfectly compatible for all hydrogen atoms (Table 4).

In NMR spectra, chemical shifts for aromatic carbons are observed in the region of 100–150 ppm [43]. The ^{13}C–NMR signals of the 2,6–DBrN molecule are experimentally in the range of 133.125–120.189 ppm. Of these values, the chemical shift values of the carbons attached to the bromine atoms are the highest. The reason for the high chemical shifts values for these two carbon atoms is that these atoms bond with the bromine atoms [21]. In addıtion, the cause for the differences in the experimental and calculated values of the chemical shifts for ^{1}H and ^{13}C atoms in the NMR spectra is the presence of intermolecular hydrogen bonding [44]. When we look at the chemical shift values for all these carbon atoms in Table 4, the experimental and calculated values seem quite compatible. When we look at the theoretical NMR chemical shift results for four different basis sets of title molecule, it is seen that the basis sets closest to the experimental result are cc-pVDZ and cc-pVTZ. It was observed that there were differences from the experimental values in the other two basis sets (6-31G(d,p) and 6-311G(d,p)). That is, the results obtained with the cc-pVDZ and cc-pVTZ basis sets are more in line with the experimental results (Table 4). This may be due to the fact that these basis sets are more suitable in terms of electron density for the atoms in the title molecule.

4.4. Natural bond orbital analysis

Another method required to examine the intermolecular interaction and bond interaction between bonds in molecules is Natural Bond Orbital (NBO) analysis. This analysis also investigates and interprets the charge transfers or conjugative interaction in the molecule [20]. In their study, James et al. reported some electron donor and acceptor orbitals and the stabilization energy resulting from the second-order micro disturbance theory [45].

For the 2,6–DBrN molecule, these energy values were calculated and tabulated with the B3LYP/cc-pVDZ basis set by the second order perturbation theory for the interaction between filled "i" and empty "j" orbitals (Table S5). In this study, we used NBO 3.1 program [46] to understand and interpret electron acceptor and donor orbitals and interactions between these orbitals.

The stabilization energy $E^{(2)}$ associated with delocalization i → j for each transmitter (i) and receiver (j) is based on the following proportion.

$$E^{(2)} = \Delta E_{ij} = q_i \frac{F(i,j)^2}{\left(\varepsilon_j - \varepsilon_i\right)}$$

where, the q_i donor is the orbital occupancy rate, ε_j, ε_i diagonal elements and $F(i,j)$ are off–diagonal NBO Fock matrix elements [21].

High conjugated interactions are formed by the overlap orbital between $\pi(C-C)$ bond orbital and $\pi^*(C-C)$ anti-bond orbital, resulting in intra-molecular load transfer that causes the system to stabilize. These interactions can be identified by finding an increase in electron density in anti-bond orbitals. According to our calculations, the double bond donor in the 2,6-Dibromonaphthalene molecule is more stable than:

$\pi(C-C) \rightarrow \pi^*(C-C)$

$\sigma(C-C) \rightarrow \sigma^*(C-C)$

$\sigma(C-C) \rightarrow \sigma^*(C-H)$

$\sigma(C-C) \rightarrow \sigma^*(C-Br)$

As can be seen in Table S5, the strongest bond interactions with the stabilization energy value of 221.21 *kJ/mol* are between $\pi(C_1-C_2) \rightarrow \pi^*(C_3-C_4)$ and $\pi(C_{10}-C_{13}) \rightarrow \pi^*(C_3-C_4)$ bonds.

The bonds and the stabilization energy values for other strong interactions calculated are given Table S5. There are also cases where the hyper conjugative interaction between some bond and anti-bond orbitals is at low stabilization energy: $\sigma(C_6-H_{12}) \rightarrow \sigma^*(C_1-C_6)$, $\sigma(C_{14}-C_{16}) \rightarrow \sigma^*(C_{13}-C_{14})$, $\sigma(H_7-C_9) \rightarrow \sigma^*(C_3-C_9)$ and $\sigma(H_7-C_9) \rightarrow \sigma^*(C_9-C_{14})$. These energy values are given in Table S5 as 0.73 *kJ/mol*, 0, 86 *kJ/mol* and 1.23 *kJ/mol*, respectively. The bond electrons here are dispersed into anti-bonds to contribute to the energy of stabilization [21].

In addition, as a result of interactions of the lone pair stabilization energy participation values are 10.18 *kJ/mol* ($LP(3)\ Br_{17} - \pi^*(C_{10}-C_{13})$ and $LP(3)\ Br_{18} - \pi^*(C_1-C_2)$).

4.5. Molecular electrostatic potential (MEP) maps

One way to find the reactivity of the point charges close to organic molecules to the regions most likely to approach these molecules is the MEP maps technique. A MEP map also provides a simple way to estimate how different geometries can interact and whether they can make links, and where to do. So these maps help to interpret the interactions between the molecule of interest and other molecules (Fig. 8(a)) [47]. Electrostatic potential counter maps are 3-dimensional diagrams that show the charge distribution in molecules. These diagrams allow us to see the size and shape of the molecule in order to understand the molecular structure [44]. Also, the molecular electrostatic potential (MEP) is related to total electron density (TED) surface (Fig. 8(b)). TED surfaces are used to locate atoms and to understand the relationships of electron densities with chemical bonds. In addition, thanks to the electron density, positive and negative potential regions in the molecule can be observed [44]. The MEP maps provide information about the electrophilic and nucleophilic reactions of the regions as well as the hydrogen bond interactions in the molecule [48]. In MEP maps, positive regions (blue) relate to nucleophilic reactivity and negative regions (red) to electrophilic reactivity. In other words, different values of electrostatic potentials on the MEP surface are represented by different colors (Fig. 8(c)). The regions in red, blue and green colors on the maps represent negative, positive and zero electrostatic potential regions, respectively. The negative electrostatic potential (red) corresponds to the withdrawal of the proton with the total electron density of the molecule, and the positive electrostatic potential (blue) refers to the proton being pushed by the atomic nucleus [49]. Also, the color codes on these maps show the blue strongest pull and red the strongest push.

In title molecule, these codes range from $-6.906 \cdot 10^{-2}$ to $6.906 \cdot 10^{-2}$. In Fig. 8, the MEP maps calculated and drawn on the cc-pVDZ basis set in the B3LYP method for the 2,6–DBrN molecule are seen from various angles. Here, for the 2,6–DBrN molecule, (a) figure shows Molecular Electrostatic Potential (MEP) Counter, (b) figure shows Total Electron Density (TED) Surface and (c) figure shows Molecular Electrostatic Potential (MEP) Surface. In the three-dimensional MEP surface, the red regions are negatively charged and the blue regions are positively charged. Negative regions are those that are far from the bromine atoms where the benzene rings intersect. This molecule can bond with other chemical compounds or groups from positively charged blue zones. In addition, color code values are in harmony with previous MEP maps [21,47].

4.6. HOMO - LUMO analysis

The frontier orbitals belonging to molecules, which are very important in quantum chemistry and quantum mechanics, can be given as the highest-occupied molecular orbitals (HOMO) and the

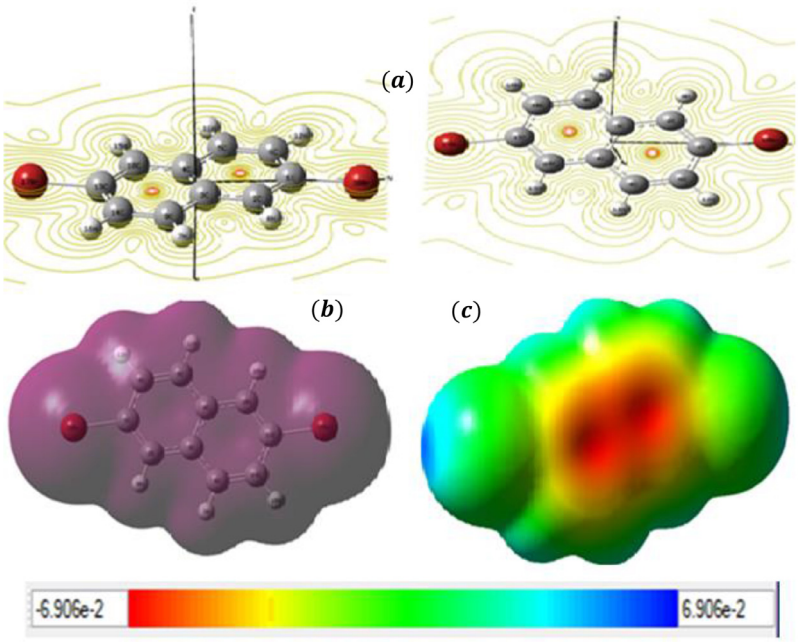

Fig. 8. MEP map views of 2,6–dibromonaphthalene molecule from various angles.
(a) molecular electrostatic potential (MEP) counter, (b) total electron density (TED) surface and (c) molecular electrostatic potential (MEP) surface.

lowest-unoccupied molecular orbitals (LUMO). While the HOMO energy of the molecule is related to its ionization potential, LUMO energy is related to electron affinity [24,25].

The gap between HOMO and LUMO energy values is defined as the chemical stability of the molecule [50]. The closer these orbital levels in the molecules are to each other, the easier the interaction between molecules. That is, a low energy gap means that the molecule is less stable [48]. Also, these orbitals in the molecules play important roles in UV/Visible spectra, chemical reactions, electrical and optical properties [51].

An electronic transition from the HOMO boundary molecular orbital to the LUMO boundary molecular orbital in molecules can be described as an electron excitation. This transition is from the base electronic level to the first excited electronic level.

The three-dimensional The HOMO, HOMO–1 and LUMO, LUMO+1 molecular orbitals energy values of the 2,6–DBrN molecule were calculated in the cc-pVDZ basis set of the B3LYP method and drawn in Fig. 9. In this molecule, HOMO is located where bromine atoms are located, and LUMO is located around the rest of the molecule, the naphthalene molecule. This means that when the HOMO–LUMO transition occurs, the electron density is transferred from the Br atoms to the naphthalene molecule. According to calculations, the energy band gap between the ground state and the first excited levels of this molecule is around 2.067 *eV*. If the molecule is stimulated again by HOMO–LUMO, the calculated value is around 3.438 *eV*. Since the difference between HOMO–LUMO energy levels is 2.067 eV in title molecule, the stability of 2,6–DBrN is low [48]. In a naphthalene derivative study, the energy difference in HOMO and LUMO levels is given as 3.81 eV [52]. This study is a study with a more stable molecule than title molecule. The reason why the molecule is stable is that it has a highly fringed structure.

4.7. Electronic absorption (UV/Visible) spectra

The UV spectrum analysis of 2,6–DBrN molecule was made by using theoretical calculations in dimethylsulfoxide (DMSO) solvent. These calculations were made using the Guassian09 package program on the basis sets TD-DFT/B3LYP/cc-pVDZ, cc-pVTZ 6-31G, and 6-311G. In this way, their excited states were determined by considering the ground state structure of the optimized 2,6–DBrN molecule. As a result of the theoretical study, absorption wavelengths (λ, nm), excitation energies (E,eV), oscillator powers (f) and transitions, so electronic values, for the 2,6–DBrN molecule are listed in Table S6 for four method/basis sets. The experimental UV/Visible spectrum of the 2,6–DBrN molecule is given in Fig. S10,(a). In this spectrum, the maximum wavelength absorbed by the molecule was observed as 249 nm. In addition, as a result of these theoretical studies, theoretical-UV spectra were drawn with the data obtained from the cc-pDVZ, cc-pTVZ, 6-31G and 6-311G basis sets and are given in Fig. S10 (b–e).

Previous studies have also shown that the wavelengths of the maximum absorption bands in the electronic spectra of such molecules vary between 200 and 320 nm. Also, the molecular orbital geometry calculations show that the apparent absorption maximum values of the molecules correspond to electron transitions between the frontier orbitals corresponding to such HOMO–LUMO energies [34,53,54]. As seen in Table S6, the theoretically calculated maximum absorption values in DMSO solvent were found as 304.83, 282.84 and 241.96 nm (at cc-pVDZ basis set), 299.66, 276.68 and 244.03 nm (at cc-pVTZ basis set), 289.83, 271.37 and 235.60 nm (at 6-31G basis set) and 282.98, 268.22 and 239.54 nm (at 6-311G basis set). These theoretical values obtained as a result of our studies correspond to $\pi - \pi^*$ transitions, which are quite compatible with the experimental maximum value. Wavelength values were found for three different transitions in theoretical calculations. One wavelength value, which is the average of the wavelength values corresponding to these transitions, may be observed in the experimental spectrum. This may also be due to the separation power of the spectrometer from which the experimental spectrum was drawn.

The following results were obtained according to the selected method/basis set for the minimum energy conformations (*atomic unit*) and zero point vibrational energy values (*kcal/mol*) of the title molecule:

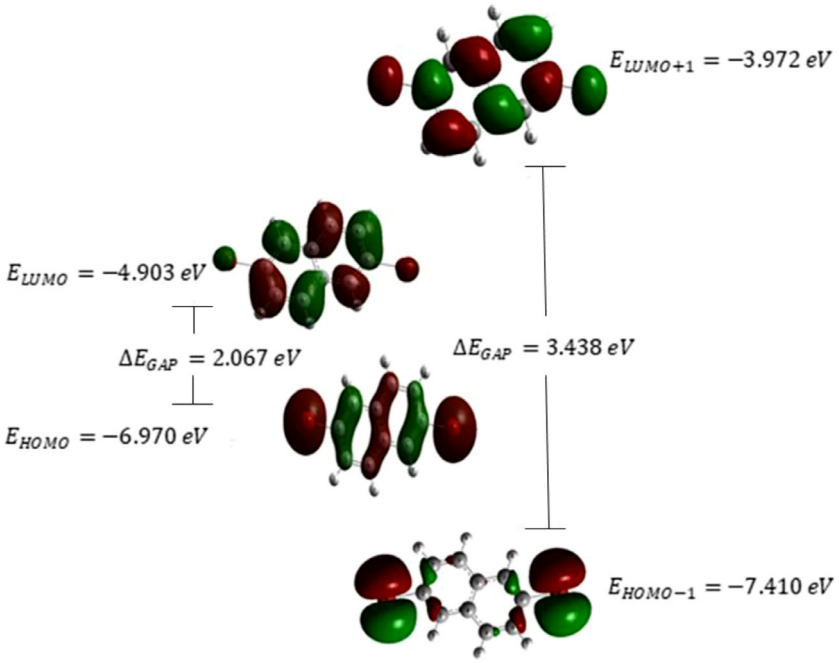

Fig. 9. Three-dimensional graph of the HOMO and LUMO orbitals of the 2,6–dibromonaphthalene molecule.

–5533.02224689 *a.u.* and 79.5463 *kcal/mol* in B3LYP / cc–pVDZ basis set,

–5533.27634905 *a.u.* and 79.5941 *kcal/mol* in B3LYP / cc–pVTZ basis set,

–5528.11157673 *a.u.* and 79.9926 *kcal/mol* in B3LYP / 6–31G(d,p) basis set

–5533.06910797 *a.u.* and 79.3099 *kcal/mol* in B3LYP / 6–311G(d,p) basis set.

From here, the decrease of the fundamental energy is due to the increase of the fundamental sets in the same group; conclusion can be reached.

5. Conclusion

In the experimental part of this study, experimental data were obtained by taking the FT–IR spectrum, FT–Raman spectrum, NMR spectrum and UV/Visible spectrum of the 2,6–dibromonaphthalene molecule. In the theoretical work part, the geometric structure of the molecule, the vibration modes, and the theoretical studies of the experimental spectra mentioned above were done with Density Function Theory (DFT). The geometric structure of the 2,6–DBrN molecule was examined in detail in theoretical and experimental manner. As a result of these investigations, the most prominent geometric parameter values, the bond length between chlorine and bromine atoms, were calculated in angstrom units as follows. The length between C_1-Br_{18} atoms: 1.916 on the cc-pVDZ basis set, 1.911 on the cc-pVTZ basis set, 1.911 on the 6-31G(d,p) basis set, and 1.917 on the 6-311G(d,p) basis set. The length between C_{13}–Br_{17} atoms: 1.916 on the cc-pVDZ basis set, 1.911 on the cc-pVTZ basis set, 1.911 on the 6-31G(d,p) basis set, and 1.917 on the 6-311G(d,p) basis set. When we look at the vibration spectra of 2,6–DBrN molecule, the C–H stretching vibration frequencies that we calculated theoretically 3119–3045 cm^{-1} are quite compatible with the frequency values in the reference articles, and they were observed in two different values in the experimental spectra (3056 cm^{-1} in FT–IR, 3052 cm^{-1} in FT–Raman). After these calculations, three-dimensional maps of the charge density of the electron were drawn using the DFT model (MEP). From the color codes on these maps, it was concluded that blue shows the strongest pull and red shows the strongest repulsion. Thus, comments were made about the molecule. Then, NBO analysis was performed on optimized structures to better understand intermolecular-interlink interactions and load transfers or conjugate interactions in molecular systems. To study the interaction of this molecule with other molecules, the $\Delta E_{HOMO-LUMO}$ energy range was also calculated with the HOMO–LUMO study. These calculations are an important study for quantum chemistry and provided information about electron transitions. Finally, the experimental and theoretical studies of the UV/Visible spectrum describing the electronic transitions that shed light on the HOMO–LUMO transitions of the molecule were compared. The maximum absorbed wavelength (λ_{max}) of title molecule in the experimental UV/Visible spectrum was found to be 249 nm. When we look at the theoretical UV/Visible spectra of this molecule, it is seen that the closest value to the experimental result is in the cc-pDTZ basis set. As a result, the data obtained by the experimental methods of the 2,6–DBrN molecule and the theoretically calculated data were compared and it was observed that these results were quite compatible.

Declaration of Competing Interest

None.

Acknowledgement

Thank you to Kırşehir Ahi Evran University Scientific Research Projects unit, which supports us in the supply of 2,6–dibromonaphthalene molecule (Project Number : PYO-FEN.4003.12.006).

Supplementary materials

Supplementary material associated with this article can be found, in the online version, at doi:10.1016/j.molstruc.2021.131834.

References

[1] T.N. Rekha, M. Umadevi, B.J.M. Rajkumar, Structural and spectroscopic study of adsorption of naphthalene on silver, J. Mol. Struct. 1079 (2015) 155–162, doi:10.1016/j.molstruc.2014.09.022.

[2] V.P. Papageorgiou, A.N. Assimopoulou, E.A. Couladouros, D. Hepworth, K.C. Nicolaou, The chemistry and biology of alkannin, shikonin, and related naphthazarin natural products, Angew. Chem. Int. 38 (1999) 270–301 10.1002/(SICI)1521-3773(19990201)38:3≤270::AID-ANIE270≥3.0.CO;2-0.

[3] L. Sun, Z. Liang, J. Yu, Octavinylsilsesquioxane-based luminescent nanoporous inorganic–organic hybrid polymers constructed by the Heck coupling reaction, Polym. Chem. 6 (2015) 917–924, doi:10.1039/C4PY01284D.

[4] H.W. Lee, H.J. Kim, Y.S. Kim, Emitting materials based on phenylanthracene-substituted naphthalene derivatives for organic light-emitting diodes, J. Lumin. 165 (2015) 99–104, doi:10.1016/j.jlumin.2015.04.029.

[5] W. Chen, T. Liu, X. Sun, et al., Facile synthesis of simple arylamine-substituted naphthalene derivatives as hole-transporting materials for efficient and stable perovskite solar cells, J. Power Sources 425 (2019) 87–93, doi:10.1016/j.jpowsour.2019.03.050.

[6] P. Kurzep, L. Skorka, M. Zagorska, et al., New quinacridone derivatives with π-extended conjugation in central core, R. Soc.Chem 7 (2017) 8627–8632, doi:10.1039/c6ra28567h.

[7] M. Mobin, M. Rizvi, L.O. Olasunkanmi, E.E. Ebenso, Biopolymer from tragacanth gum as a green corrosion inhibitor for carbon steel in 1M HCl solution, Am. Chem. Soc. 2 (2017) 3997–4008, doi:10.1021/acsomega.7b00436.

[8] Đ. Škalamera, L. Cao, L. Isaacs, R. Glaser, K. Mlinarić-Majerski, Steric hindrance to the syntheses and stabilities of 1, 5-and 2, 6-naphthalene N-permethylated diammonium salts, Tetrahedron 72/12 (2016) 1541–1546, doi:10.1016/j.tet.2016.02.002.

[9] A. Rauf, H. Subhan, R. Abbasi, et al., Biological activity, pH dependent redox behavior and UV–Vis spectroscopic studies of naphthalene derivatives, J. Photochem. Photobiol. B 140 (2014) 173–181 http://dx.doi.org/10.1016/j.jphotobiol.2014.07.010.

[10] S. Banerjee, E.B. Veale, C.M. Phelan, et al., Recent advances in the development of 1,8-naphthalimide based DNA targeting binders, anticancer and fluorescent cellular imaging agents, Chem. Soc. Rev. 42 (2013) 1601–1618 http://pubs.rsc.org/doi:10.1039/C2CS35467E.

[11] J. Trotter, The crystal structure of 1,4-dibromonaphthalene, Can. J. Chem. 39 (1961) 1574–1578.

[12] R.C. Haltiwanger, P.T. Beurskens, J.M.J. Vankan, W.S. Veeman, Crystal structure of 1,5-dibromonaphthalene and of disordered 1,8-dibromonaphthalene, J. Crystallogr. Spectrosc. Reserach. 14 (1984) 589–597.

[13] X.-X. Wu, Y. Wan, S.W. Ng, 3,6-Di-bromo-naphthalene-2,7-diylbis-(tri-fluoro-methane-sulfonate), Acta Cryst. E67 (2011) 2698, doi:10.1107/S1600536811037755.

[14] K. Geeta, M. Umadevi, G.V. Sathe, R. Erenler, Spectroscopic investigations on the orientation of 1,4-dibromonaphthalene on silver nanoparticles, Spectrochim. Acta A 116 (2013) 236–241, doi:10.1016/j.saa.2013.07.039.

[15] A.L. McClellan, G.C. Pimentel, Vibrational assignment and thermodynamic properties of naphthalene, J. Chem. Phys. 23 (1955) 245–248, doi:10.1063/1.1741948.

[16] E.R. Lippincott, E.J. O'Reilly Jr., Vibrational Spectra and assignment of naphthalene and naphthalene-D-8, J. Chem. Phys. 23 (1955) 238–244, doi:10.1063/1.1741947.

[17] K.H. Michaelian, S.M. Ziegler, Vibrational spectra and assignments for series of mono- and dihalonaphthalenes, Appl. Spectrosc. 27 (1) (1973) 13–21, doi:10.1366/000370273774333966.

[18] L. Lohmeyer, E. Kaifer, H. Wadepohl, H.-J. Himmel, 1,2,5,6-Tetrakis(guanidino)-naphthalenes: electron donors, fluorescent probes and redox-active ligands, Chem. A Eur. J. 26 (2020) 5834–5845 /26, doi:10.1002/chem.201905471.

[19] M.J. Frisch, G.W. Trucks, H.B. Schlegel, G.E. Scuseria, M.A. Robb, J.R. Cheesemen, et al., Gaussian09, Revision A.2, Gaussian, Inc., Wallingford CT, 2009.

[20] P. Pulay, J. Baker, K. Wolinski, Green acres road suite A fayettevile, Arkansas 72703, USA, 2013.

[21] E.B. Sas, M. Kurt, M. Karabacak, A. Poiyamozhi, N. Sundaraganesan, FT-IR, FT-Raman, dispersive Raman, NMR spectroscopic studies and NBO analysis of 2-Bromo-1H-Benzimidazol by density functional method, J. Mol. Struct. 1081 (2015) 506–518, doi:10.1016/j.molstruc.2014.10.025.

[22] G. Gece, The use of quantum chemical methods in corrosion inhibitor studies, Corros. Sci. (2008).

[23] K. Fukui, Theory of Orientation and Stereo Selection, Springer-Verlag, Berlin, 1975.

[24] F. Fleming, Frontier Orbitals and Organic Chemical Reactions, John Wiley and Sons, New York, 1976.

[25] T. Yesilkaynak, G. Binzet, F.M. Emen, U. Flörke, N. Külcü, H. Arslan, Theoretical and experimental studies on N-(6-methylpyridin-2-yl-carbamothioyl)biphenyl-4-carboxamide, Eur J. Chem. 1 (1) (2010) 1–5, doi:10.5155/eurjchem.1.1.1-5.3.

[26] R. Ditchfield, Molecular orbital theory of magnetic shielding and magnetic susceptibility, J. Chem. Phys. 56 (1972) 5688–5691, doi:10.1063/1.1677088.

[27] K. Wolinski, J.F. Hinton, P. Pulay, Efficient implementation of the gauge-independent atomic orbital method for NMR chemical shift calculations, J. Am. Chem. Soc. 112/23 (1990) 8251–8260, doi:10.1021/ja00179a005.

[28] S. Subashchandrabose, A.R. Krishnan, H. Saleem, V. Thanikachalam, G. Manikandan, Y. Erdogdu, FT-IR, FT-Raman, NMR spectral analysis and theoretical NBO, HOMO–LUMO analysis of bis(4-amino-5-mercapto-1,2,4-triazol-3-yl)ethane by ab initio HF and DFT methods, J. Mol. Struct. 981 (2010) 59–70, doi:10.1016/j.molstruc.2010.07.025.

[29] P. Udhayakala, A. Jayanthi, T.V. Rajendiran, S. Gunasekaran, Molecular structure, FT-IR and FT-Raman spectra and HOMO-LUMO analysis of 2-methoxy-4-nitroaniline using ab initio HF and DFT (B3LYP/B3PW91) calculations, Arch. Appl. Sci. Res. 3 (4) (2011) 424–439 http://scholarsresearchlibrary.com/archive.html.

[30] A. Fu, D. Du, Z. Zhou, Density functional theory study of vibrational spectra of acridine and phenazine, Spectrochim. Acta A 59 (2) (2003) 245–253, doi:10.1016/S1386-1425(02)00169-5.

[31] R.M. Silverstein, F.X. Webster, D.J. Kiemle, Spectrometric Identification of Organic Compounds, John Wiley&Sons, 2015.

[32] M. Karabacak, M. Kurt, A. Ataç, Experimental and theoretical FT-IR and FT-Raman spectroscopic analysis of N1-methyl-2-chloroaniline, J. Phys. Org. Chem. 22 (4) (2009) 312–330, doi:10.1002/poc.1480.

[33] N. Sundaraganesan, H. Saleem, S. Mohan, Vibrational spectra, assignments and normal coordinate analysis of 3-aminobenzyl alcohol, Spectrochim. Acta. A 59 (11) (2003) 2511–2517, doi:10.1016/S1386-1425(03)00037-4.

[34] B.H. Stuart, Infrared Spectroscopy, Fundamentals and Applications, Wiley, 2004.

[35] E.H. Avdović, D.S. Dimić, M. Fronc, J. Kožišek, E. Klein, Ž.B. Milovanović, A. Kesić, Z.S. Marković, Structural and theoretical analysis, molecular docking/dynamics investigation of 3-(1-m-chloridoethylidene)-chromane-2,4-dione: the role of chlorine atom, J. Mol. Struct. 1231 (2021) 129962, doi:10.1016/j.molstruc.2021.129962.

[36] G. Varsayni, Assignments of Vibrational Spectra of Seven Hundred Benz1ene Derivatives, 1-2, Adamm Hilger, 1974.

[37] N. Sundaraganesan, H. Saleem, S. Mohan, M. Ramalingam, V. Sethuraman, FTIR, FT-Raman spectra and ab initio DFT vibrational analysis of 2-bromo-4-methylphenylamine, Spectrochim. Acta A 62A (2005) 740–751, doi:10.1016/j.saa.2005.02.043.

[38] M.A. Iramain, A.E. Ledesma, S.A. Brandan, Structural properties and vibrational analysis of Potassium 5-Br-2-isonicotinoyltrifluoroborate salt. Effect of Br on the isonicotinoyl ring, J Mol. Struct. 1184 (2019) 146–156, doi:10.1016/j.molstruc.2019.02.010.

[39] M.E. Manzur, S.A. Brandán, S(-) and R(+) species derived from antihistaminic promethazine agent: structural and vibrational studies, Heliyon 5 (2019) e02322, doi:10.1016/j.heliyon.2019.e02322.

[40] N. Sundaraganesan, S. Ilakiamani, H. Saleem, P.M. Wojciechowski, D. Michalska, FT-Raman and FT-IR spectra, vibrational assignments and density functional studies of 5-bromo-2-nitropyridine, Spectrochim. Acta A 61A (2005) 2995–3001, doi:10.1016/j.saa.2004.11.016.

[41] N. Subramanian, N. Sundaraganesan, J. Jayabharathi, Molecular structure, spectroscopic (FT-IR, FT-Raman, NMR, UV) studies and first-order molecular hyperpolarizabilities of 1,2-bis(3-methoxy-4-hydroxybenzylidene)hydrazine by density functional method, Spectrochim. Acta A 76A (2010) 259–269, doi:10.1016/j.saa.2010.03.033.

[42] M. Karabacak, Z. Calisir, M. Kurt, E. Kose, A. Atac, The spectroscopic (FT-IR, FT-Raman, dispersive Raman and NMR) study of ethyl-6-chloronicotinate molecule by combined density functional theory, Spectrochim. Acta A 153A (2016) 754–770, doi:10.1016/j.saa.2015.09.007.

[43] H.O. Kaiinowski, S. Berger, S. Braun, Carbon-13 NMR Spectroscopy, John Wiley & Sons, Chichester, 1988.

[44] S. Muthu, E.E. Porchelvi, FTIR, FT-Raman, NMR, spectra,normal co-ordinate analysis, NBO, NLO and DFT calculation of N,N-diethyl-4-methylpiperazine-1-carboxamide molecule, Spectrochim. Acta A 115 (2013) 275–286 http://dx.doi.org/10.1016/j.saa.2013.06.011.

[45] C. James, A. Amal Raj, R. Reghunathan, V.S. JayaKumar, I. Hubert Joe, Structural conformation and vibrational spectroscopic studies of 2,6-bis(p-N,N-dimethyl benzylidene)cyclohexanone using density functional theory, J. Raman Spectrosc. 37 (12) (2006) 1381–1392, doi:10.1002/jrs.1554.

[46] E.D. Glendening, C.R. Landis, F. Weinhold, in: Comput. Mol. Sci, John Wiley & Sons. Ltd. WIREs, 2011, pp. 1–42.

[47] T.R. Sertbakan, Structure, spectroscopic and quantum chemical investigations of 4-amino-2-methyl-8-(trifluoromethyl)quinoline, Celal Bayar Univ. J. Sci. 13 (4) (2017) 851–861, doi:10.18466/cbayarfbe.339858.

[48] M.G. Diego, M.E. Defonsi Lestard, O.E. Hernandes, J. Dugue, E. Reguera, Quantum chemical studies on molecular structure, spectroscopic (IR, Raman, UV–Vis), NBO and Homo–Lumo analysis of 1-benzyl-3-(2-furoyl) thiourea, Spectrochim. Acta A 145A (2015) 553–562, doi:10.1016/j.saa.2015.02.071.

[49] F. Fleming, Frontier Orbitals and Organic Chemical Reactions, John Wiley and Sons, New York, 1976.

[50] R. Gupta, A.K. Gupta, S. Paul, Microwave-assisted synthesis and biological activities of some 7/9-substituted-4-(3-alkyl/aryl-5,6-dihydro-s-triazolo[3,4-b][1,3,4]thiadiazol-6-yl)tetrazolo[1,5-a]quinolines, Indian J. Chem. 39B (2000) 847–852.

[51] E. Kavitha, N. Sundaraganesan, S. Sebastian, M. Kurt, Molecular structure, anharmonic vibrational frequencies and NBO analysis of naphthalene acetic acid by density functional theory calculations, Spectrochim. Acta A 77A (2010) 612–619, doi:10.1016/j.saa.2010.06.034.

[52] M. Genç, The synthesis, characterization and Gaussian calculations of N-(4-methylphenyl)-N-(5-(3-hydroxynahptyl-2-yl)-1,3,4-oxadiazol-2-yl)amine, Iğdır Univ, J. Inst. Sci. & Tech. 8 (1) (2018) 169–177, doi:10.21597/jist.407866.
[53] D. Dimić, D. Milenković, J. Ilić, B. Šmit, A. Amić, Z. Marković, J.D. Marković, Experimental and theoretical elucidation of structural and antioxidant properties of vanillylmandelic acid and its carboxylate anion, Spectrochim. Acta A 198 (2018) 61–70, doi:10.1016/j.saa.2018.02.063.
[54] Ž.B. Milanović, Z.S. Marković, D.S. Dimić, O.R. Klisurić, I.D. Radojević, D.S. Šeklić, M.N. Živanović, J.D. Marković, M. Radulović, E.H. Avdović, Synthesis, structural characterization, biological activity and molecular docking study of 4,7-dihydroxycoumarin modified by aminophenol derivatives, C. R. Chim. 24 (2) (2021) 215–232, doi:10.5802/crchim.68.